A Boundary Integral Method for Computing Eddy Currents in Non-Manifold Thin Conductors

Paolo Bettini[1,2], Paweł Dłotko[3], and Ruben Specogna[4]

[1]Dipartimento di Ingegneria Industriale, Università di Padua, Padua 35131, Italy
[2]Consorzio RFX, Padua 35127, Italy
[3]Inria Saclay, Palaiseau 91120, France
[4]Dipartimento di Ingegneria Elettrica Gestionale e Meccanica, Università di Udine, Udine 33100, Italy

We introduce a novel technique to solve eddy current problems in non-manifold thin conductors by a boundary integral method based on a stream function. The idea is to perform a surgery on the non-manifold surface representing the thin conductor to reduce it into a minimal number of manifold parts. Then, manifold parts are stitched together by adding constraints, which ensure that the discrete current continuity law holds.

***Index Terms*—Eddy currents, integral methods, non-manifold geometry, thin shields, topological surgery.**

I. Introduction

THE boundary integral method (BIM) represents a thin conductor as a 2-D surface. Here, this approach is used to model a conductor whose thickness δ is small with respect to the penetration depth of the magnetic field. In this case, the induced current density can be considered as uniform in the conductor thickness, and it can be modeled by a stream function [1]. Nonetheless, we remark that a stream function may also be used for problems with arbitrary skin depth [2].

Recently, an effective technique to render the stream function single valued based on the computation of relative cohomology generators in linear worst case complexity has been introduced [3]. This algorithm, contrarily to some others published in literature, is able to find the required relative cohomology generators for an arbitrary orientable discrete surface, i.e., technically a combinatorial orientable 2-manifold with boundary embedded in $\mathbb{R}^3$ [4].

Moreover, almost all papers assume the thin conductor to be an orientable 2-manifold, in most cases without saying it. As far as we know, how to extend the BIM to deal with non-manifold geometries is discussed only in [1] and [5], still without the necessary details. For example, how to automatically partition the geometry such that each partition is a manifold and a topological disk—as required by [1]—is non-trivial and left completely unaddressed in [1] and [5]. Also, how to write the constraints in the case of non-trivial topology is not discussed in detail.

The aim of this contribution is to present an original recipe to generalize the use of the BIM to most non-manifold geometries (a more precise definition of most is presented in Section III).

This paper is organized as follows. In Section II, we briefly present the BIM for manifold surfaces. This novel presentation, although equivalent in practice to the one described in [3], renders the extension of BIM to non-manifold surfaces as painlessly as possible. Section III shows how potential has to be redefined when dealing with non-manifold surfaces. Section IV introduces the novel formulation and some details on the practical implementation. Finally, Section V shows the results on a number of benchmark problems.

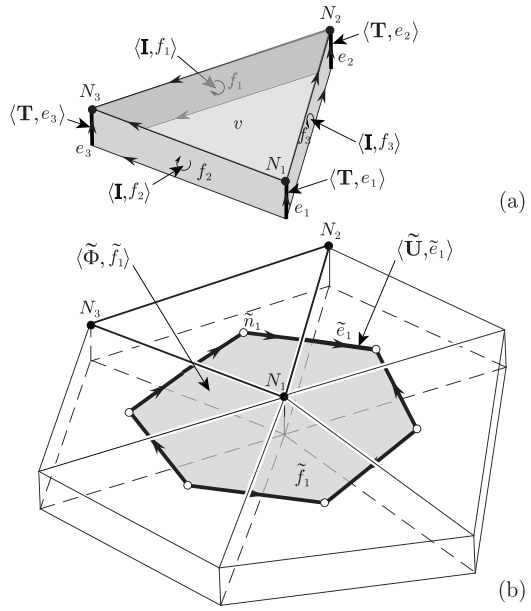

Fig. 1. Association of physical variables to geometric elements of (a) primal and (b) dual complexes.

II. BIM for Manifold Surfaces

The discrete surface is constructed as a conformal mesh formed by N nodes $\{N_i\}_{i=1}^{N}$, E edges $\{E_j\}_{j=1}^{E}$, and P polygons $\{P_k\}_{k=1}^{P}$. From the mesh, the primal cell complex $\mathcal{K}$ [6] is constructed as follows, see Fig. 1(a). The elements are defined as rectangular prisms $\{v_i\}_{i=1}^{P}$ constructed by considering the polygons with a thickness δ, see Fig. 1(a). Faces $\{f_i\}_{i=1}^{E}$ are defined as the lateral faces of the prisms (one-to-one with the

Manuscript received July 3, 2015; accepted September 1, 2015. Date of publication September 4, 2015; date of current version February 17, 2016. Corresponding author: P. Bettini (e-mail: paolo.bettini@unipd.it).

Color versions of one or more of the figures in this paper are available online at http://ieeexplore.ieee.org.

Digital Object Identifier 10.1109/TMAG.2015.2476841

mesh edges), and edges $\{e_i\}_{i=1}^{N}$ are those normal to the symmetry plane (one-to-one with the mesh nodes), see Fig. 1(a). Then, the dual nodes $\tilde{n}$, dual edges $\tilde{e}$, and dual faces $\tilde{f}$ belonging to the dual complex $\tilde{\mathcal{K}}$ are constructed. They are obtained from $\mathcal{K}$ with the standard barycentric subdivision [6], see Fig. 1(b). Interconnections of the geometric elements of the primal and dual complex are given in terms of usual incidence matrices. We consider the incidence matrices $\mathbf{C}$ between pairs (f, e), $\tilde{\mathbf{C}}$ between pairs $(\tilde{f}, \tilde{e})$, in regard to which $\tilde{\mathbf{C}} = \mathbf{C}^T$ holds [6], and $\mathbf{D}$ between pairs (v, f).

We associate an unknown current on faces $f_i \in \mathcal{K} - \partial\mathcal{K}$, whereas we assume that there is no current on boundary faces to prevent current flowing outside the conducting shell. Such unknown currents are the coefficients of the 2-cochain $\mathbf{I}$. We denote the coefficient of an arbitrary cochain $\mathbf{c}$ corresponding to the geometric element e as $\langle \mathbf{c}, e \rangle$.

Since $\mathbf{I}$ is a 2-cocycle [7], [9], i.e., $\mathbf{DI} = \mathbf{0}$, it can be represented by

$$\mathbf{I} = \mathbf{CT} + \mathbf{Hi} \tag{1}$$

where $\mathbf{T}$ is the potential 1-cochain, $\mathbf{i}$ is the array of *independent currents* [7], and the columns of $\mathbf{H}$ store the representatives of $H^2(\mathcal{K} - \partial\mathcal{K})$ generators [9]. Concerning boundary conditions, the coefficients of $\mathbf{T}$ on edges and on $\partial\mathcal{K}$ should be set to zero. Moreover, if some connected components of $\mathcal{K}$ do not have boundaries, $\mathbf{T}$ on one arbitrary edge of each of such connected components has to be fixed to zero. The boundary conditions are also the very reason why relative cohomology $H^2(\mathcal{K}-\partial\mathcal{K})$ is needed in place of the absolute one $H^2(\mathcal{K})$.

Then, we enforce the discrete Faraday's law on the boundary of dual faces that are dual to interior edges with

$$\mathbf{C}^T\tilde{\mathbf{U}} + i\omega\tilde{\boldsymbol{\Phi}} = -i\omega\mathbf{C}^T\tilde{\mathbf{A}}_s \tag{2}$$

where $\tilde{\mathbf{U}}$ is the electromotive force (EMF) on dual edges, $\tilde{\boldsymbol{\Phi}}$ is the magnetic flux produced by eddy currents on dual faces and $\tilde{\mathbf{A}}_s$ is the circulation of the magnetic vector potential due to the source currents on dual edges. The two constitutive laws are expressed in the discrete setting as

$$\tilde{\mathbf{U}} = \mathbf{RI} \quad \text{and} \quad \tilde{\mathbf{A}} = \mathbf{MI} \tag{3}$$

where $\mathbf{R}$ and $\mathbf{M}$ are the classical resistance mass matrix and the magnetic matrix [1], respectively. By substituting (1), (3), and $\tilde{\boldsymbol{\Phi}} = \mathbf{C}^T\tilde{\mathbf{A}}$ inside (2) and by defining $\mathbf{K} = \mathbf{R} + i\omega\mathbf{M}$

$$(\mathbf{C}^T\mathbf{KC})\mathbf{T} + (\mathbf{C}^T\mathbf{KH})\mathbf{i} = -i\omega\mathbf{C}^T\tilde{\mathbf{A}}_s. \tag{4}$$

Yet, EMFs evaluated on non-trivial elements of $H_1(\tilde{\mathcal{K}}) \simeq H^2(\mathcal{K} - \partial\mathcal{K})$ are still undetermined, since they cannot be spanned by a linear combination of the boundaries of dual faces. Hence, non-local Faraday's laws enforced on a basis of $H_1(\tilde{\mathcal{K}})$ have to be added

$$(\mathbf{H}^T\mathbf{KC})\mathbf{T} + (\mathbf{H}^T\mathbf{KH})\mathbf{i} = -i\omega\mathbf{H}^T\tilde{\mathbf{A}}_s. \tag{5}$$

III. Non-Manifold Surface Surgery

In Section II, we treated the case of manifold discrete surfaces. In this section, we start from a non-manifold surface and perform a surgery on it in such a way that the ideas from the previous section can be used again.

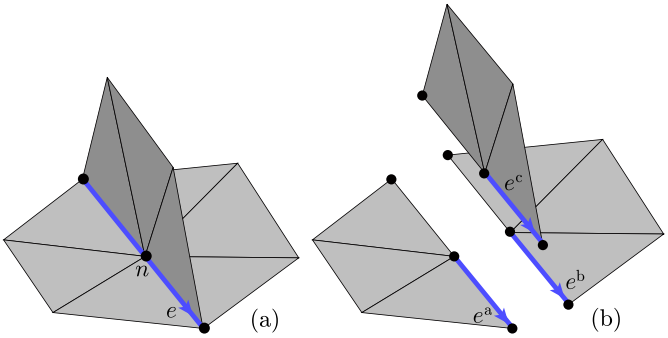

Fig. 2. (a) Non-manifold discrete surface $\mathcal{S}$. Non-manifold edges, as e, and non-manifold nodes are marked. (b) $\mathcal{S}$ is cut into a minimal number of manifold parts. The manifold parts are drawn exploded for clarity, but the coordinates of the triplicated nodes are inherited from the original node.

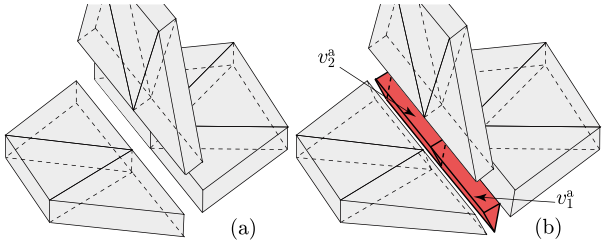

Fig. 3. (a) Primal complex of each manifold part is constructed independently. Again, manifold parts are drawn exploded for clarity. (b) Manifold parts are stitched back together by adding prismatic volumes as v_1^a and v_2^a.

Let us denote by $\mathcal{E}$ the set of non-manifold edges of the non-manifold surface $\mathcal{S}$, i.e., the edges where more than two faces of the mesh meet. An example of such a surface $\mathcal{S}$ is visible in Fig. 2(a). In Fig. 2(a), edge e is non-manifold as it is incidental to three triangles.

We perform a surgery on $\mathcal{S}$ by separating it into a minimal number of manifold parts as follows. The original mesh is partitioned into pieces such that each piece is a manifold and the edges in $\mathcal{E}$ can appear only on the boundary of each piece. For example, we consider the case where three manifold surfaces join together, as in Fig. 2(a). To construct the modified mesh, we first triplicate the non-manifold edges and nodes and update the incidence matrices accordingly, as in Fig. 2(b). Second, we require the triplicated edges e^a, e^b, and e^c to have the same orientation as the original edge e, see Fig. 2(b). Finally, we also isoorient all 2-D elements on each manifold part. This is performed by fixing the orientation of a random polygon on each manifold part and by iteratively orienting the others accordingly with a standard breadth-first search technique [8].

Then, the primal complex of each manifold part is constructed exactly as in the manifold case. The obtained primal complex for the example is shown in Fig. 3(a).

We have now to stitch back together the manifold parts taking care that the discrete current continuity law holds where they join. This is performed by adding one prismatic element for each original non-manifold edge where current conservativity has to be imposed as in any other primal element. v_1^a and v_2^a in Fig. 3(b) are the prismatic elements

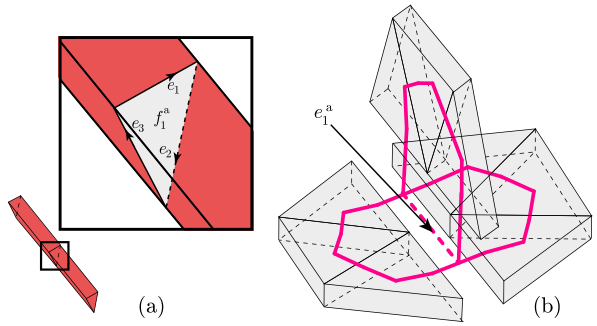

Fig. 4. (a) Two prisms v_1^a and v_2^a and a zoomed-in view on the additional face f_1^a. (b) Dual complex $\tilde{\mathcal{K}}$ comprises the additional dual edge e_1^a, which is dual to f_1^a (the two prisms v_1^a and v_2^a are not shown in this picture for clarity).

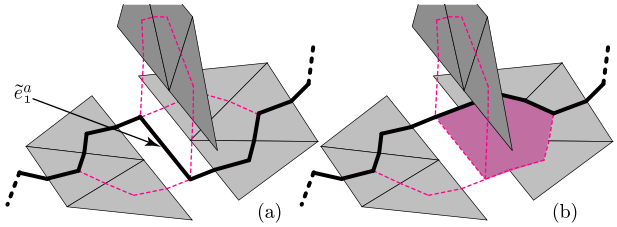

Fig. 5. (a) Support of the representative of the $H_1(\tilde{\mathcal{K}})$ generator computed automatically crosses the additional dual edge $\tilde{e}_1^a$. (b) Another representative in the same homology class is obtained by summing the highlighted dual face to the previous generator.

to be added in the example. Let us call the obtained primal complex $\mathcal{K}$.

To define potentials, we have to update (1). In fact, other faces internal to $\mathcal{K}$ are present apart the usual primal faces $\{f_i\}_{i=1}^E$, see f_1^a in Fig. 4(a). Those are in one-to-one correspondence with non-manifold nodes and not edges $\{E_j\}_{j=1}^E$ as f_i. We have to set the current over additional faces as f_1^a to zero. Referring to face f_1^a of Fig. 4(a)

$$\langle \mathbf{T}, e_1 \rangle + \langle \mathbf{T}, e_2 \rangle + \langle \mathbf{T}, e_3 \rangle = 0 \tag{6}$$

have to be added to (1), where e_1, e_2, and e_3 are the primal edges in the boundary of the additional face f_1^a. All these constraints, one for each additional face, are collected together as $\mathbf{NT} = \mathbf{0}$. The boundary conditions on $\mathbf{T}$ are enforced exactly as in the manifold case.

The dual complex $\tilde{\mathcal{K}}$ is constructed as usual. It features an additional dual edge e_1^a, which is dual to the additional face f_1^a, see Fig. 4(b). These additional dual edges play a role in the formulation as—like any other dual edge—they have EMFs associated with them. These new unknowns EMFs correspond to the new constraints (6). This means we have to update Faraday's laws (2), since the boundary of some dual faces also comprises the contribution of EMFs on the additional dual edges as e_1^a. Faraday's laws on $\tilde{\mathcal{K}}$ become

$$\mathbf{C}^T \tilde{\mathbf{U}} + \mathbf{W} \tilde{\mathbf{U}}^a + i\omega \tilde{\boldsymbol{\Phi}} = -i\omega \mathbf{C}^T \tilde{\mathbf{A}}_s \tag{7}$$

where matrix $\mathbf{W}$ stores the incidences between the additional dual edges and the dual faces and $\tilde{\mathbf{U}}^a$ are the additional unknowns EMFs.

Similarly to the manifold case, when the domain is topologically non-trivial, non-local Faraday's equations on the generators of $H_1(\tilde{\mathcal{K}})$ have to be added. One may compute $H_1(\tilde{\mathcal{K}})$ generators in negligible time by standard techniques that compute homology over $\mathbb{Z}_2$. However, the support of such generators may intersect some additional dual edges, as in Fig. 5(a). We must avoid such a case, since we want the dual of $H_1(\tilde{\mathcal{K}})$ generators not to include additional faces as f_1^a in Fig. 4(a). In fact, we required by (1) that the currents over such faces to be zero and we cannot, therefore, have those faces in the support of the cohomology generators. This, in turn, means that the representatives of $H_1(\tilde{\mathcal{K}})$ generators have to be post-processed to avoid additional dual edges in their support.

The post-processing of generators is quite easy and it is performed, as Fig. 5 suggests, by adding to the generator—for each additional dual edge $\tilde{e}_1^a$ crossed—the boundaries of one of the dual faces incident to $\tilde{e}_1^a$ (Fig. 5). Since we add boundaries to generators, this clearly cannot change their homology class. Moreover, since the homology computation is performed on $\mathbb{Z}_2$, the coefficients of the cycle representing the generator can be only zero or ± 1, which shows the generality of the procedure.

Finally, the dual of such representatives of generators is used to construct the column of matrix $\mathbf{H}$. Since these are relative cohomology $H^2(\mathcal{K} - \partial\mathcal{K})$ generators of the primal complex $\mathcal{K}$, current continuity law and Ampère's law hold.

We remark that one may compute the relative $H^2(\mathcal{K} - \partial\mathcal{K})$ cohomology generators directly and then apply a similar post-processing to them to avoid additional faces. This is, however, not convenient, as it requires us to explicitly produce the 3-D primal complex $\mathcal{K}$. On the contrary, the dual complex required by $H_1(\tilde{\mathcal{K}})$ can be easily constructed in practice.

IV. Novel Formulation

To obtain a symmetric system, that is $\mathbf{W} = \mathbf{N}^T$, all incidences inside $\mathbf{W}$ must be one. This simply implies a constraint on the normal of each manifold part. Practically, we first fix a random orientation for the first manifold part, and then orient all others making sure that the orientation of the additional dual edge in the corresponding dual face to be one. We remark that if there is some non-orientable part like a Möbius band embedded in the non-manifold surface, one cannot orient all manifold parts consistently and the software exits notifying the user about this problem. Therefore, this remark answers the question of which non-manifold surface we can deal with.

The final system to solve is then

$$\begin{bmatrix} \mathbf{C}^T\mathbf{K}\mathbf{C} & \mathbf{C}^T\mathbf{K}\mathbf{H} & \mathbf{N}^T \\ \mathbf{H}^T\mathbf{K}\mathbf{C} & \mathbf{H}^T\mathbf{K}\mathbf{H} & \mathbf{0} \\ \mathbf{N} & \mathbf{0} & \mathbf{0} \end{bmatrix} \begin{bmatrix} \mathbf{T} \\ \mathbf{i} \\ \tilde{\mathbf{U}}^a \end{bmatrix} = \begin{bmatrix} -i\omega\mathbf{C}^T\tilde{\mathbf{A}}_s \\ -i\omega\mathbf{H}^T\tilde{\mathbf{A}}_s \\ \mathbf{0} \end{bmatrix}. \tag{8}$$

V. Numerical Results

The proposed approach has been applied to calculate the currents induced in a non-manifold thin conducting structure by external ac fields. First, a 3-D problem with cylindrical

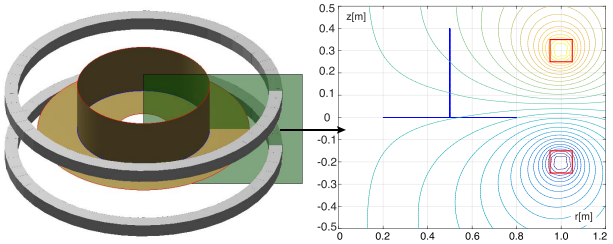

Fig. 6. Left: 3-D problem with cylindrical symmetry. A conducting structure (uniform resistivity $\rho = 0.1\ \mu\Omega$ and thickness $\delta = 1$ mm) placed in the region between a pair of coils. Right: 2-D view. The magnetic field produced by the coils (ac current, $f = 50$ Hz, anti-series connected) is also shown.

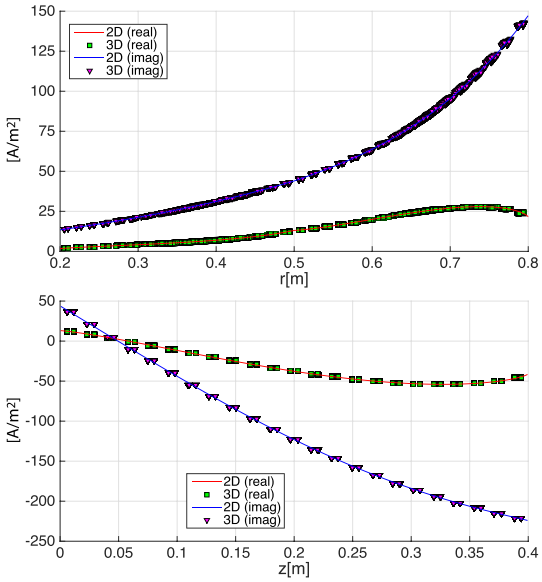

Fig. 7. 3-D solution versus 2-D: real and imaginary parts of the current density (J_ϕ component) induced in the drilled disk (top—$z = 0$ m and $r = 0.2 \div 0.8$ m) and in the cylinder (bottom—$r = 0.5$ m and $z = 0 \div 0.4$ m).

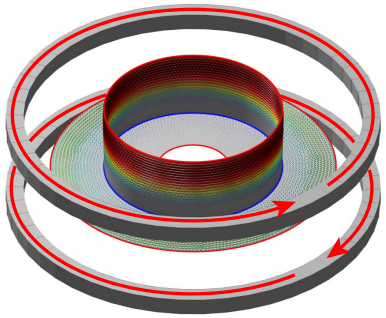

Fig. 8. 3-D solution of the problem shown in Fig. 6. The conducting structure is discretized with 17 144 triangles, 26 187 edges, and 9043 nodes (157 non-manifold). Colored cones: real part of the induced current density. The hotter the color, the higher the current density.

symmetry has been considered (see Fig. 6). The 3-D solution is compared with the reference one, calculated on a fine 2-D mesh (see Fig. 7). An excellent agreement is found in terms

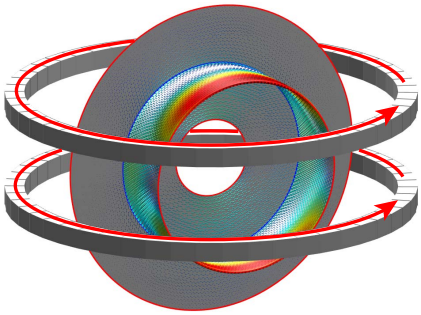

Fig. 9. 3-D (non-axisymmetric) current density pattern induced by two circular loops (ac current, $f = 50$ Hz) series connected. Colored cones: real part of the current density. The hotter the color, the higher the current density.

of both real and imaginary components of the current density induced in the two manifold parts, the drilled disk and the cylinder. The 3-D current density pattern is shown in Fig. 8. Then, the same conducting structure is immersed in the field produced by the same pair of loops, but 90° rotated and series connected. The 3-D current density pattern is shown in Fig. 9.

ACKNOWLEDGMENT

This work was supported by the Foundation of Polish Science Start Scholarship.

REFERENCES

[1] A. Kameari, "Transient eddy current analysis on thin conductors with arbitrary connections and shapes," *J. Comput. Phys.*, vol. 42, no. 1, pp. 124–140, Jul. 1981.

[2] T.-T. Nguyen, G. Meunier, J.-M. Guichon, and O. Chadebec, "3-D integral formulation using facet elements for thin conductive shells coupled with an external circuit," *IEEE Trans. Magn.*, vol. 51, no. 3, Mar. 2015, Art. ID 6300504.

[3] P. Bettini and R. Specogna, "A boundary integral method for computing eddy currents in thin conductors of arbitrary topology," *IEEE Trans. Magn.*, vol. 51, no. 3, Mar. 2015, Art. ID 7203904.

[4] K. Itō, *Encyclopedic Dictionary of Mathematics*, 2nd ed. Cambridge, MA, USA: MIT Press, 1987.

[5] A. V. Belov *et al.*, "Transient electromagnetic analysis in tokamaks using typhoon code," *Fusion Eng. Design*, vol. 31, no. 2, pp. 167–180, Jun. 1996.

[6] E. Tonti, "A direct discrete formulation of field laws: The cell method," *CMES, Comput. Model. Eng. Sci.*, vol. 2, no. 2, pp. 237–258, 2001.

[7] P. Dłotko and R. Specogna, "Physics inspired algorithms for (co)homology computations of three-dimensional combinatorial manifolds with boundary," *Comput. Phys. Commun.*, vol. 184, no. 10, pp. 2257–2266, Oct. 2013.

[8] T. H. Cormen, C. E. Leiserson, R. L. Rivest, and C. Stein, *Introduction to Algorithms*, 2nd ed. Cambridge, MA, USA: MIT Press, 2001.

[9] J. R. Munkres, *Elements of Algebraic Topology*. New York, NY, USA: Perseus Books, 1984.